2

UCRL- JC-113742
PREPRINT

DUAL-BAND INFRARED THERMOGRAPHY FOR QUANTITATIVE NONDESTRUCTIVE EVALUATION

P.F. Durbin, N.K. Del Grande, K.W. Dolan,
D.E. Perkins and A.B. Shapiro

This paper was prepared for submittal to
the 1993 JANNAF Nondestructive Evaluation
Subcommittee Meeting, Livermore, CA
April 26-28, 1993

April 1993

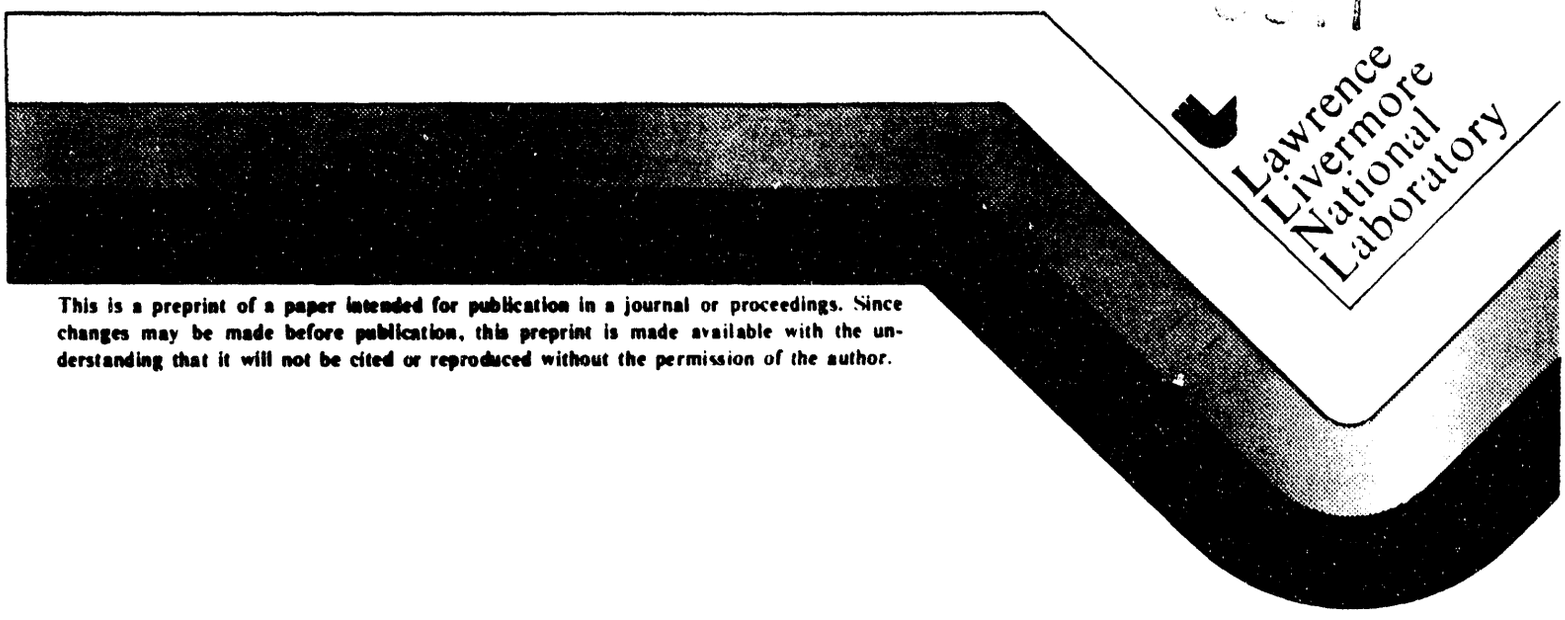

DISCLAIMER

DUAL-BAND INFRARED THERMOGRAPHY FOR QUANTITATIVE NONDESTRUCTIVE EVALUATION *

P.F. Durbin, N.K. Del Grande, K.W. Dolan,
D.E. Perkins and A.B. Shapiro
Lawrence Livermore National Laboratory
P.O. Box 808, Livermore, CA 94550

ABSTRACT

We have developed dual-band infrared (DBIR) thermography that is being applied to quantitative nondestructive evaluation (NDE) of aging aircraft. The DBIR technique resolves 0.2 degrees C surface temperature differences for inspecting interior flaws in heated aircraft structures. It locates cracks, corrosion sites, disbonds or delaminations in metallic laps and composite patches. By removing clutter from surface roughness effects, we clarify interpretation of subsurface flaws. To accomplish this, we ratio images recorded at two infrared bands, centered near 5 microns and 10 microns. These image ratios are used to decouple temperature patterns associated with interior flaw sites from spatially varying surface emissivity noise. We also discuss three-dimensional (3D) dynamic thermal imaging of structural flaws using dual-band infrared (DBIR) computed tomography. Conventional thermography provides single-band infrared images which are difficult to interpret. Standard procedures yield imprecise (or qualitative) information about subsurface flaw sites which are typically masked by surface clutter. We use a DBIR imaging technique pioneered at LLNL to capture the time history of surface temperature difference patterns for flash-heated targets. We relate these patterns to the location, size, shape and depth of subsurface flaws. We have demonstrated temperature accuracies of 0.2 °C, timing synchronization of 3 ms (after onset of heat flash) and intervals of 42 ms, between images, during an 8 s cooling (and heating) interval characterizing the front (and back) surface temperature-time history of an epoxy-glue disbond site in a flash-heated aluminum lap joint.

INTRODUCTION

Previous LLNL applications of the precise airborne temperature survey for imaging and detection of underground and obscured object sites have depicted heat flow anomalies which produced distinguishable surface temperature differences from:

(a) geothermal aquifers under 6 to 60 meters of dry soil
(b) cemetery walls, trenches and building foundations under 80 cm of asphalt and debris,
(c) buried mines, rocks and objects under 1 to 20 cm of disturbed sand, soil, or sod
(d) sea ice thicknesses varying from 5 to 50 cm.

Current applications of DBIR imaging sponsored by the FAA Technical Center are to develop DBIR imaging for nondestructive inspection (NDI) of heated aircraft parts tested in a laboratory environment. We have imaged the following sites of:

(a) subsurface corrosion in F-111 wing panels from McClellan AFB
(b) delaminations in aircraft composite patches developed by Northrop Corporation,
(c) disbonds in aluminum lap joints made by Boeing

We are presently evaluating a new sensitive IR imaging work station that is being configured as a DBIR unit. With this equipment measuring temperature differences smaller than 0.1 degree C should be possible.

Applying thermal modeling codes helps us understand heat flow in different types of aircraft parts Powerful codes developed at LLNL can reduce experimental time and cost. We are also developing three-dimensional dynamic thermal imaging to measure flaw depth based on thermal patterns and timing.

*Work performed under auspices of the U.S. Department of Energy by the Lawrence Livermore National Laboratory under contract No. W-7405-ENG-48.
Approved for public release; distribution unlimited

DBIR CONCEPT AND UNDERLYING PRINCIPLE

The LLNL state-of-the art DBIR technique remotely images hidden structural defects by mapping precise surface temperature-difference patterns in steps of 0.2 Celsius. In addition, it provides surface emissivity-ratio maps to reduce false detections by locating and removing clutter. Our DBIR system typically images infrared wavelength intervals of about one micron (peaked at 4.7 microns) and two microns (peaked at 10.6 microns).

The DBIR thermal imaging technique uses simultaneous recording of two passive IR bands and unique correction algorithms to decouple temperature from surface emissivity noise. A mathematical approximation derived from Planck's Radiation Law shows that short / long wave band image ratios map surface temperature patterns depicting subsurface object sites. The $(\text{long})^2$ / short wave band image ratios map surface emissivity patterns from clutter. This method exploits the dependence of radiant emittance signals on surface temperature to the power 50 / (wavelength in microns) at temperatures near 288 Kelvin.

Defects in aircraft parts heat and cool at different rates than the defect-free parts which surround them. A similar principle of heat transfer through materials with different thermal properties allowed us to detect buried land mines covered by 1 to 15 cm of soil.

POWER LAW MODEL

A power law model [1-4] explains how infrared signals vary as a function of the surface emissivity and the surface's absolute temperature:

$$I_\lambda \sim e_\lambda T^{50/\lambda} \quad , \tag{1}$$

where I_λ is the intensity at a given wavelength, e_λ is emissivity at that wavelength, T is in temperature in Kelvin and λ is the wavelength in micrometers.

We can obtain temperature alone by computing the ratio

$$R = \frac{I_5}{I_{10}} = \frac{e_5 T^{50/5}}{e_{10} T^{50/10}} = \frac{e_5}{e_{10}} T^5 \quad , \tag{2}$$

For a greybody, $e_5 = e_{10}$, $R \sim T^5$.

We can obtain the emissivity ratio by computing

$$\frac{(I_{10})^2}{I_5} = \frac{(e_{10})^2 (T^5)^2}{e_5 T^{10}} = \frac{(e_{10})^2}{e_5} \tag{3}$$

This ratio is sensitive mostly to surface objects which have very different emissivities at 5 and 10 micrometers (most metal surfaces).

We then compute the normalized ratios to obtain temperature and emissivity-ratio (E-ratio) maps:

$$T = \ln \frac{S/S_{av}}{L/L_{av}} \text{ and E-ratio } = \ln \frac{(L/L_{av})^2}{S/S_{av}} \tag{4}$$

where S is the short-wavelength intensity (e.g., I_5), S_{av} is the average value of the pixels in S, L is the long wavelength intensity (e.g., I_{10}) and L_{av} is the average value of the pixels in L.

Several other corrections are also applied to the DBIR scanner signals (e.g., for absorption and reemission in the air path between the scanner and the surface, and for reflected infrared (IR) radiation. [2,3,4]

INFRARED COMPUTED TOMOGRAPHY

We expect infrared computed tomography to be achievable with resources developed at LLNL for other applications. By synchronizing the heat source (such as a series of flash lamps) with the Agema 880 DBIR camera and digital image processing system we recorded and processed images taken at intervals of 42 ms. Surface thermal patterns have spatial and time variations that characterize the location, size and depth of subsurface defects in the host material. Calculations based on the TOPAZ 3D heat transfer model and other models developed for x-ray and gamma-ray computed tomography (CT) will be used to reconstruct 3D images of structural defects. We are addressing the inherent problems associated with single-band dynamic thermal tomography using the DBIR technique.

To identify small temperature differences from weak heat flow anomalies at the sites of deep structural defects, one must first remove the order of magnitude larger apparent temperature differences from surface emissivity noise. There are no algorithms able to do this for a single-band system. The alternative is elaborate surface preparation (using paint, paper or powder). This raises the sensitivity threshold for weak heat flow detection.

The DBIR imaging technique provides a factor of ten better temperature-difference sensitivity, accuracy and precision. This technique offers improved image clarity and interpretability when we use ratios of 5 and 10 μm IR images to remove clutter and enhance thermal contrast. In addition, the DBIR method maps corrected temperature patterns (associated with weak heat flow anomalies at defect sites) and removes spatially varying surface emissivity noise (associated with surface roughness differences, coating discontinuities or other, inhomogeneous effects).

THERMAL MODELING OF HEATED AIRCRAFT PARTS

Thermal modeling (i.e. computer simulation) is a cost-effective way to investigate the sensitivity of an experimental measurement to system variables which affect the measurement (e.g. surface conditions, material properties, crack size). Additionally, thermal modeling gives insight into the accuracy ranges required for sensors, location of the sensors on the work piece, and inspection strategies. We use TOPAZ as the thermal modeling computer code. TOPAZ can solve problems of surface diffuse and specular band radiation coupled with conduction in the body. Additionally, TOPAZ can model conduction and radiation heat transfer across internal gaps. Material properties may be temperature dependent and either isotropic or orthotropic. A variety of time or temperature dependent boundary conditions can be specified including temperature, flux convection and radiation.

USE OF TOPAZ3D MODEL

Thermal analysis of the lap joint test specimen was performed using TOPAZ3D [5]. TOPAZ3D is a three-dimensional implicit finite element computer code for transient or steady state heat transfer analysis. A variety of time or temperature dependent boundary conditions may be specified, including temperature, flux, convection, and radiation. Material properties may be temperature dependent and either isotropic or orthotropic. TOPAZ3D has been extensively used at LLNL for more than a decade.

The flash-lamp heat pulse is approximated as a constant heat flux applied uniformly over the front surface of the test specimen. The time for heating is 4.2 ms which corresponds to the duration of the flash-lamp pulse in the experiment, however we realize that the actual flash pulse is neither constant nor uniform. In determining the magnitude of the applied flux we had to estimate the absorptance of the test specimen and the fraction of emitted flash-lamp light which reaches the test specimen. Radiation and convection heat losses to the environment are included in the calculation. We have confidence in the accuracy of the temperature field calculated by TOPAZ3D. The TOPAZ3D result for the peak front surface temperature compared well with the temperature calculated from a 1-D closed-form solution. [6] In addition, the finite element mesh was refined to show that convergence had been reached. The penetration depth of the

flash-lamp heating pulse into the aluminum plate (during heating) was determined to be 60 mils (0.06 inches) at the end of the pulse. [5]

TOPAZ3D results are shown later in the text for comparison with measurement. We simulate an experiment where two flash lamps were used to illuminate the test specimen, whose surfaces had been coated with black paint to enhance absorptivity. The trend of the simulation result parallels the trend of the experimental data quite well.

DBIR TECHNIQUE TO FIND HIDDEN FLAWS IN AIRCRAFT PARTS

Laboratory tests of the DBIR imaging technique were conducted for flaw detection of aircraft parts as part of the FAA Tech Center Aging Aircraft Program. We describe our results for a composite patch and aluminum lap joint. Currently, We use the digitized SWB and LWB infrared images recorded with the Agema 880 DBIR camera system and Burst Recording Unit (BRU) as input to a Silicon Graphics Inc. (SGI) Workstation. This procedure provides apparent temperature images recorded at wavelengths centered near 10 μm (LWB) and 5 μm (SWB), for comparison with temperature map images derived from Equation (2) and emissivity-ratio map images derived from Equation (3).

LABORATORY DEMONSTRATION

Composite patches made of advanced materials (e.g., thermoplastics obtained from Northrop Corporation) are expected to play an important role for aircraft repair. We are investigating a variety of heat sources and inspection methods. This allows us to correlate the results we obtain with the DBIR technique with those obtained with other methods.

Patch. The DBIR technique provides high thermal sensitivity for aircraft structural inspection by decoupling spatially dependent emissivity noise from true thermal images. This greatly improves the signal to noise ratio, thereby clarifying interpretation of hidden defect sites which produce time-varying surface thermal "footprints".The composite patch was inspected with ultrasonic testing (UT) methods both at Northrop and at Lawrence Livermore Laboratories. The center of the patch appears less flawed than the outer two rings at the top of Figure 1a & b. This is confirmed by the thermal image in Figure 2 and the temperature histogram in Figure 3. The temperature histogram of a region near the patch shows a central zone (with the hottest surface temperatures) and a smaller substrate zone (with the coldest surface temperatures) which sandwich uneven temperature distributions associated with the outer two rings of the oven-heated patch.

The similar patch results obtained using UT and DBIR methods give a synergistic advantage, often associated with sensor fusion, clarifying interpretation of hidden defects in complex composite materials. Additional synergy is provided by comparing the temperature image in Figure 2 (for a flash-heated patch, corrected to remove uneven heat source) with the temperature images in Figure 3 a,b,c (for oven-heated patch). The composite patch had near-uniform emissivity ratios (shown in Figure 3d.).

Lap-joint. In Figure 4a, we see a diagram of the lap joint. There is a rectangular (0.1 mm thick) air layer representing the disbond site. Figure 4b shows a 10 μm IR image of the disbond site the surface of which is 0.4 or 0.5 °C warmer (where it was flash heated) than the epoxy-glue sites which surround it. In Figure 4c is the ultrasound image which shows a better bond quality in the epoxy region, indicated by lower signal values (higher values to the right side of the grey scale) compared to the higher signal values in the epoxy free region.. Figure 4d shows reverse geometry x rays at 100 keV which transmit differently through two overlapping (0.5 mm thick) Al sheets which sandwich the 0.1 mm air gap than the equally thick epoxy-glue layer.

In Figure 5, we see front-surface (top images) and back-surface (bottom images) of apparent temperatures at 10 μm (a-d) and 5 μm (e-h) recorded at 0.5, 2, 4 and 8 seconds after flash-heating the front surface. The front and back images were recorded simultaneously with the 10 μm IR scanner in the front (flash lamp side) and the 5 μm IR scanner in the back. The maximum thermal contrast between air and epoxy-glue layers occurred at approximately 2 seconds. The front surface disbond site stayed warmer longer (and the back surface remained cooler longer) than ambient bonded sites because air is a good insulator. It provides a heat sink, which retains heat from the flash-heated front surface and delays heat from reaching the back surface.

In Figure 6, we note subtle differences between the lap joint apparent temperature-difference images recorded at 10 μm (a), 5 μm (b), and with DBIR image ratios which produce a temperature map enhancing thermal contrast (c). The emissivity-ratio map (d) is nearly constant, unlike the temperature maps (a), (b), and (c) for an Al target painted black to maximize heat absorptivity. Both the 10μm and the 5μm images were taken from the front (flash lamp side). We obtained about three times the thermal contrast (between air and epoxy-glue sites) using black paint rather than white powder. Most aircraft parts are expected to have surfaces which are painted or coated with sealants to impede corrosion.

Comparison of measurements with calculations. Surface temperature differences which separate air disbond sites from epoxy-glue bonded sites peak about 2 seconds after flash-heating the lap joint on the front side according to our results (see Figure 7a). A fifth order polynomial fit was made to the averaged data for air disbond and glue bond sites scanned at the front with the LWB detector and at the back with the SWB detector Figure 7b). The two detectors were synchronized with the flash unit and recorded nearly simultaneously (within 10 ms). The fifth order polynomial fits to data not shown (Figure 7b) and provided a good fit to temperature difference data (Figure 7a) and the time derivative of temperature data (Figure 7c).

Calculations of early response data are shown in Figure 8 together with the front surface and back surface air minus glue site temperature differences. There appears to be agreement between calculation and measurement, but further refinement is needed to improve the input parameters for the TOPAZ3D model.

SUMMARY AND CONCLUSIONS

We demonstrated the capability of the DBIR technique to precisely locate weak heat flow anomalies from a lap joint disbond site with a layer of air (0.1 mm thick) bounded above and below by bonded epoxy glue sites and sandwiched between two (0.9 mm thick) aluminum sheets. Also, we converted scaled DBIR image ratio data to temperature maps which enhance thermal contrast and emissivity-ratio maps which reject sites with surface roughness variations, coating differences and other heterogeneous effects.

The dual-band technique has the following advantages over a single band techniques:

- provides five to ten times better temperature difference accuracy and precision,
- uses image ratios to remove clutter and enhance thermal contrast,
- decouples temperature from spatially varying surface emissivity noise, and
- locates weak heat flow anomalies from subsurface flaw sites.

We used fast-captured surface temperature images to study the temperature versus time history of subsurface defect sites from a lap joint. We combined three multisensor techniques to characterize the lap-joint and patch disbond sites, namely: infrared, ultrasound and x rays. These techniques provided information about heat transfer anomalies, the bond quality and material differences at the disbond site.

We plan to use TOPAZ3D calculations to model the dynamic relationships between the flaw site surface temperature versus time and the subsurface flaw size, shape and depth. We will adapt the appropriate DBIR procedures based on our experiences which have successfully developed x-ray and gamma-ray computed tomography. These procedures will be tested to determine the three dimensional heat transfer properties which lead to circular thermal images on back surface scans of lap joint disbond sites compared to rectangular thermal images on front surface scans taken at the same time.

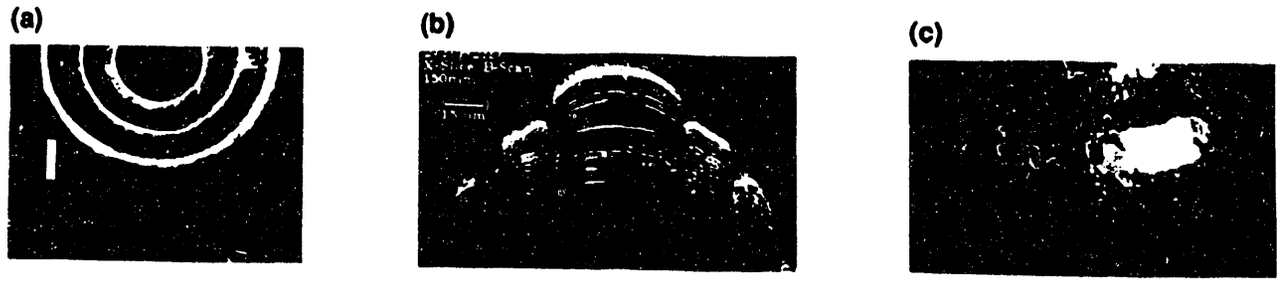

Figure 1. (a) Photo of aircraft composite patch; (b) ultrasonic testing (UT) B-scan; (c) UT C-scan.

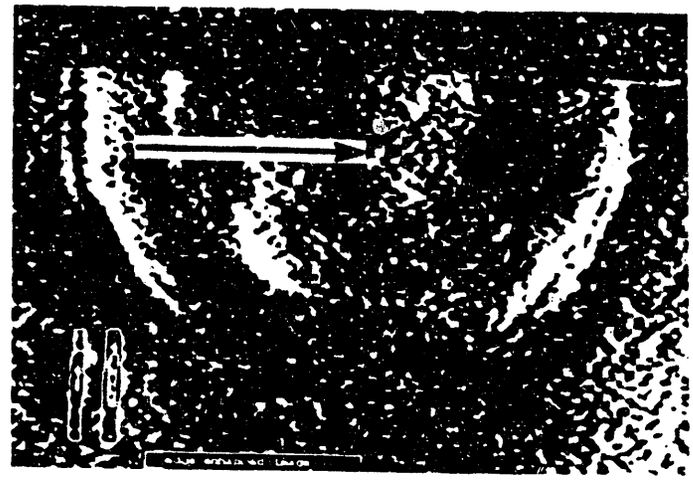

Figure 2. Composite patch edge enhancement 10 μm thermal image with arrow pointing to subsurface delamination zone at 46 seconds after front heat applied by flash lamp.

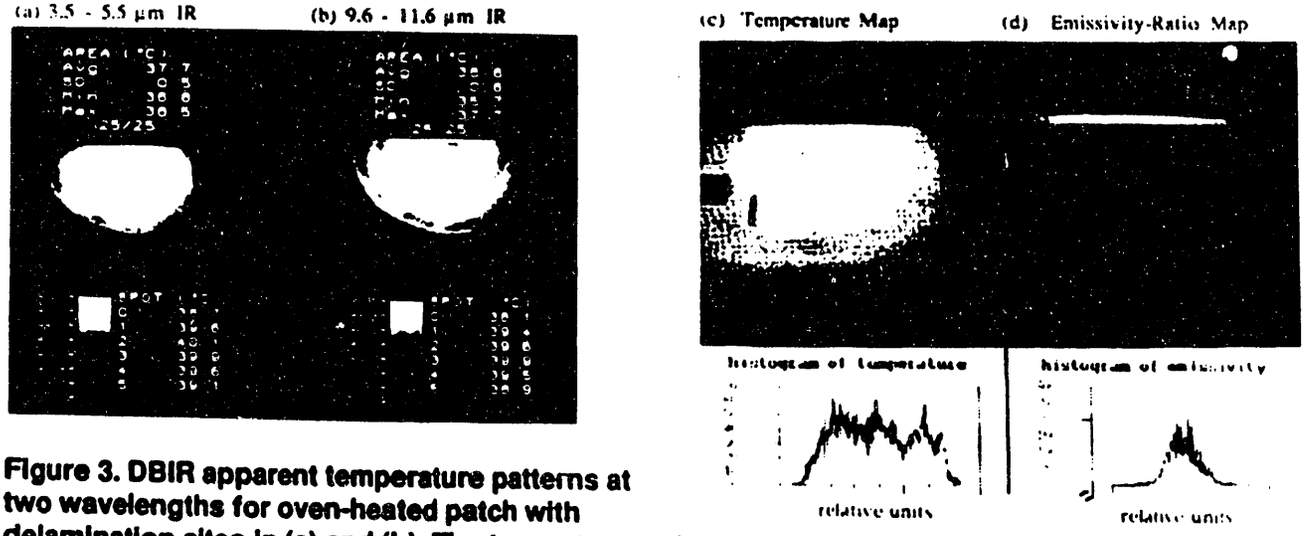

Figure 3. DBIR apparent temperature patterns at two wavelengths for oven-heated patch with delamination sites in (a) and (b). The two outer patch rings have uneven heat flow patterns in temperature map (c) and histogram below. Histogram tic mark spacings (left to right) are 0.05, 0.02, 0.05, and 0.05 respectively.

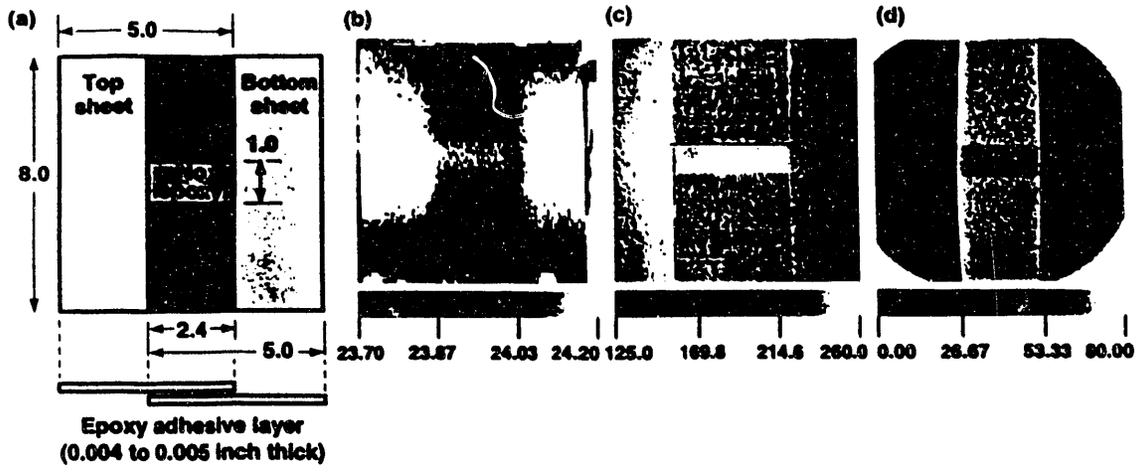

Figure 4

(a) Lap-joint
(b) Infrared
(c) Ultrasound
(d) X-ray

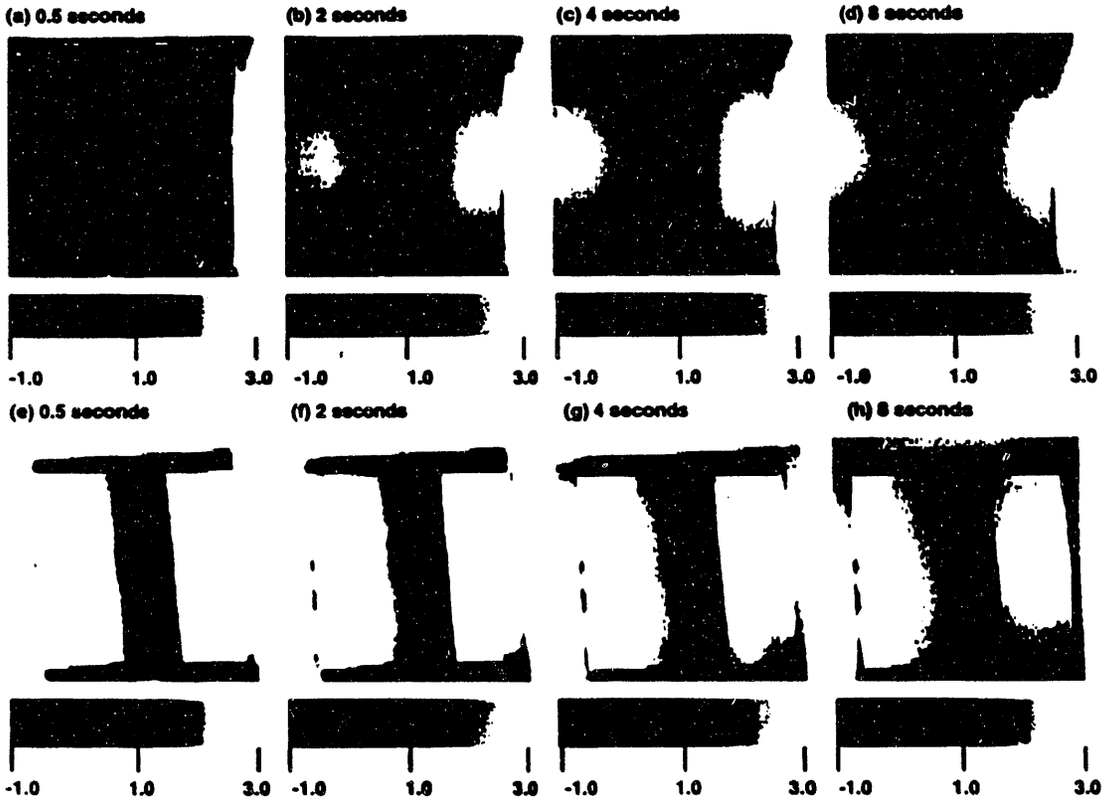

Figure 5

Top row
(a, b, c, d)
Lap-joint
front surface
temperatures,
flash lamp side

Bottom row
(e, f, g, h)
Lap-joint back
surface
temperatures

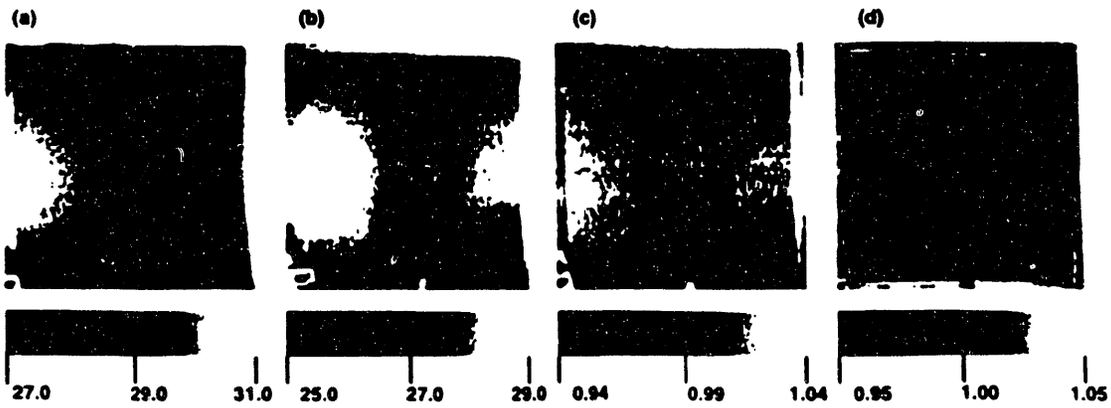

Figure 6

(a) Lap-joint 10 μm
(b) Lap-joint 5 μm
(c) Temperature map
(d) Emissivity-ratio map

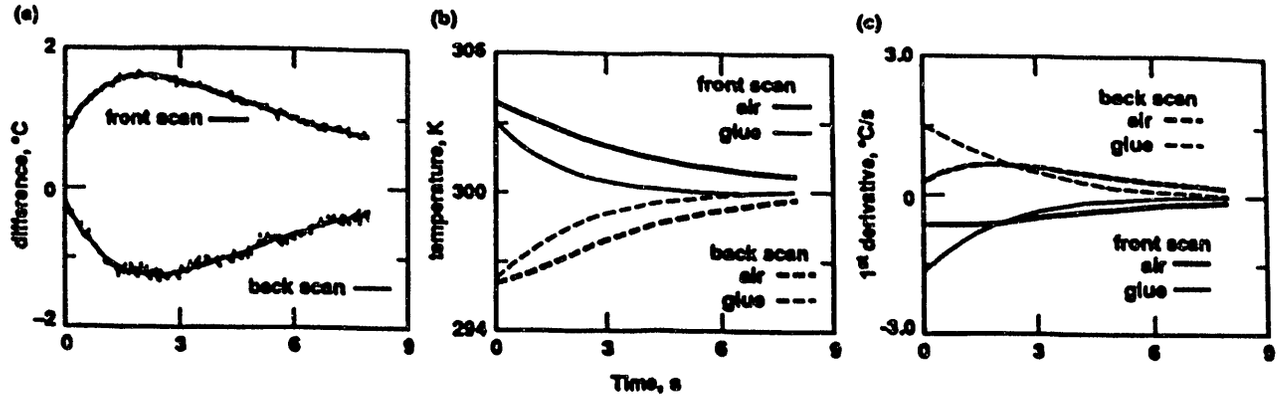

Figure 7

(a) Measured surface temperature difference between disbond site and ambient site on front and back surface

(b) Fifth order polynomial fit to apparent temperature for front and back surface data

(c) First derivative with respect to temperature for the fit curve in Figure 7b

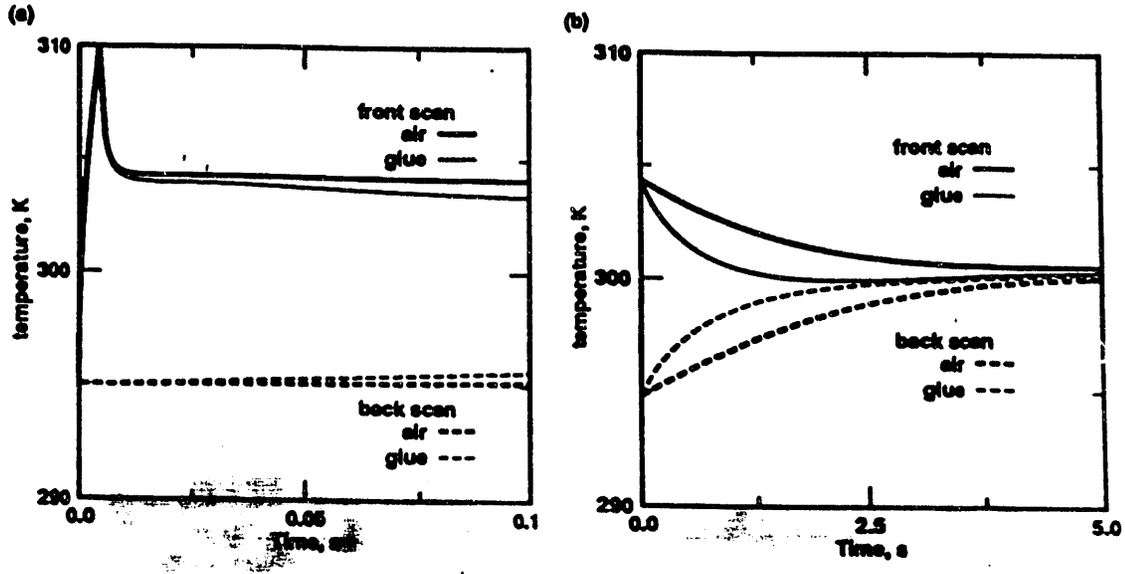

Figure 8

(a), (b) Calculations of early response data corresponding to measured data shown in Figure 7b

ACKNOWLEDGMENTS

This work was conducted by LLNL for DOE contract W-7405-ENG-48. We acknowledge the sponsorship of FAA's Aging Aircraft Program I-A Agreement DTFA03-92-A-0007; and DARPA's Countermine Program ARPA Order No. 7180-01. We wish to thank S. Kulkarni for his technical assistance and support; M. Bales for use of his IR scanner; M. Gorvad for help preparing computer processed images; B. Kornblum for thermal model analysis; O. Manning (Northrop Corporation) for the composite patch samples and S. Benson for the UT scans conducted at LLNL.

References

[1] N. K. Del Grande, G. A. Clark, P. F. Durbin, D. J. Fields, J. E. Hernandez and R. J. Sherwood, "Buried Object Remote Detection Technology for Law Enforcement" in *SPIE Vol. 1479 Surveillance Technologies*, pp. 335-351, April 1991.

[2] N. Del Grande, "Sensor Fusion Methodology for Remote Detection of Buried Land Mines" in *Proceedings of the 3rd National Symposium on Sensor Fusion, Vol. 1*, pp. 407-427, ERIM, Aug. 1990.

[3] N. Del Grande, "Temperature Evaluated Mine Position Survey (TEMPS) Application of Dual-Band Infrared Methodology Proceedings
of the 1990 Meeting of the IRIS Specialty Group on Passive Sensors, IRIA/ERIM-sponsored, Baltimore MD, March 1990.

[4] L. A. LeSchack and N. K. Del Grande "A Dual-Wavelength Thermal Infrared Scanner as a Potential Airborne Geophysical Exploration Tool", in *Geophysics 41*, p. 1318, 1976.

[5] A. B. Shapiro, "TOPAZ3D A Three Dimensional Finite Element Heat Transfer Code", University of California, Lawrence Livermore National Laboratory, Rept. UCID-20484, August 1985

[6] A. B. Shapiro and A. L. Edwards, "TOPAZ2D Heat Transfer Code Users Manual and Thermal Property Data Base"' University of California, Lawrence Livermore National Laboratory, Rept. UCRL-ID-104558, May 1990.

[7] N.K. Del Grande, P.F. Durbin and D.E. Perkins,"Dual-Band Infrared Imaging Applications: Locating Buried Minefields, Mapping Sea Ice, And Inspecting Aging Aircraft", *In Proceedings: Quantitative Nondestructive Evaluation Conference, San Diego, Ca*, July 1992 (to be published).

END

DATE FILMED

10/15/93